Quaternary International 679 (2024) 25–35

Contents lists available at ScienceDirect

Quaternary International

journal homepage: www.elsevier.com/locate/quaint

^{10}Be surface exposure dating of glacier fluctuations on the eastern slope of Mount Geladandong, central Tibetan Plateau

Jingdong Zhao [a,d,*], Jinkun Qiu [b], Jonathan M. Harbor [c], Wanqin Guo [a], Marc M. Caffee [c,e], Huihan Ji [b], Jingling Chen [a], Xiaobo He [a,f]

[a] SKLCS, Northwest Institute of Eco-Environment and Resources, Chinese Academy of Sciences, Lanzhou, Gansu, 730000, China
[b] Key Laboratory of Western China's Environmental Systems (MOE), Lanzhou University, Lanzhou, Gansu, 730000, China
[c] Department of Earth, Atmospheric, and Planetary Sciences, Purdue University, Purdue University Global, West Lafayette, IN, 47907, USA
[d] School of Geography, Geomatics, and Planning, Jiangsu Normal University, Xuzhou, Jiangsu, 221116, China
[e] Department of Physics and Astronomy, Purdue Rare Isotope Measurement Laboratory (PRIME Lab), Purdue University, West Lafayette, IN, 47907, USA
[f] Tanggula Mountain Cryosphere and Environment Observation Station, Northwest Institute of Eco-Environment and Resources, CAS, Lanzhou, Gansu, 730000, China

ARTICLE INFO

Keywords:
^{10}Be surface exposure dating
Glacial landforms
Little ice age (LIA)
Tanggula mountains
Central Tibetan Plateau (TP)

ABSTRACT

Moraine complexes formed by multiple glaciations are well-preserved in the Mount Geladandong area, the largest center of current glaciation in the Tanggula Mountains in western China. Studies of these glacial landforms provide insights into past glacier changes and contribute to understanding palaeoclimate and palaeoenvironment in the central Tibetan Plateau (TP). Here we report on ^{10}Be surface exposure dating of thirteen rock samples collected from a sequence of glacial landforms associated with the Gangjiaquba Glacier. Based on the dating results, historical records (topographical maps) and morphological relationships, clear Little Ice Age (LIA) landforms are identified, and other landforms are tentatively assigned Neoglacial and global Last Glacial Maximum (LGM_G) ages. Dating results for samples from modern glacial landforms demonstrate that the boulders were not affected by nuclide inheritance, and that ^{10}Be surface exposure dating may be used to constrain glacier fluctuations during the past century in high-altitude areas that have high ^{10}Be production rates. A comparison of the ages of a glacially polished surface and adjacent glacial deposits indicates that subglacial erosion by abrasion of the rock surface was insufficient to remove cosmogenic nuclide inventories. Thus the apparent exposure age on the polished surface includes inheritance and over-estimates the actual age for the exposure of this surface. Samples from hummocky moraine have wide age spreads, indicating long-lasting surface instability after deposition of this landform. Successive reduction in glacial extent in the Mount Geladandong area since the LGM_G reflects temperature and precipitation changes over this timeframe in the central TP, with climate forcing for glacial advances correlated with cooling signals in the North Atlantic that may have been transmitted to this area by the westerlies.

1. Introduction

Outside of the polar regions, the Tibetan Plateau (TP) and its surroundings make up the most glaciated region on Earth with the largest number of modern mountain glaciers (Yao et al., 2012). These glaciers are the source of water for many prominent Asian rivers, including the Indus, Ganges, Brahmaputra, Yangtze and Yellow (Immerzeel et al., 2010), and meltwater provides a vital resource for billions of people and has been central to the development of society, ecology and economy in Asia. Ongoing global warming has resulted in substantial loss of ice from most glaciers in this area (Guo et al., 2015; Liu et al., 2015; Jakob et al., 2021), reflected in thinning and retreat. Distinct glacial erosional and depositional landforms from multiple glaciations are widespread in valleys, basins, and on piedmonts throughout the TP and its surroundings, and prior work has shown that large-scale glacial advances and retreats occurred here during Quaternary glacial-interglacial cycles (Li et al., 1986; Shi et al., 2006, 2011). These landforms are direct imprints of palaeoglaciation and represent important archives of past climatic and environmental information. Studies of these landforms across the TP are revealing spatiotemporal variations of ancient glaciers and landscape evolution, and intraregional and interregional differences of glaciations that provide insights into variations in climate drivers across the

* Corresponding author. SKLCS, Northwest Institute of Eco-Environment and Resources, Chinese Academy of Sciences, Lanzhou, Gansu, 730000, China.
E-mail address: jdzhao@lzb.ac.cn (J. Zhao).

https://doi.org/10.1016/j.quaint.2023.12.004
Received 10 September 2023; Received in revised form 13 November 2023; Accepted 5 December 2023
Available online 12 December 2023

TP (Dortch et al., 2013; Murari et al., 2014; Owen and Dortch, 2014).

The development and refinement of numerical dating techniques applied to glacial landforms and sediments in recent decades has provided new insights into the timing, extent, and nature of Quaternary glaciations (Shi et al., 2006, 2011; Ehlers et al., 2011; Owen and Dortch, 2014), including terrestrial *in situ* cosmogenic nuclides (TCN), optically stimulated luminescence (OSL) and electron spin resonance (ESR). Refined frameworks for glaciation on the TP and its surroundings have been established, and local glacial stages have been identified and suggested (Zhao et al., 2011; Dortch et al., 2013; Murari et al., 2014). These data have also contributed to studies of possible climate forcing mechanisms and global climate change (Balco, 2020). However, the paucity of robust chronological data in the central TP is a gap that is impeding understanding paleoglaciation of this key region. More accurate and precise dating is needed to fully understand the spatiotemporal variations of palaeoglaciers and landscape evolution of the central TP.

The Tanggula Mountains are a distinct and tectonically active mountain system in the central TP (Fig. 1), trending NWW and stretching about 500 km from Mitijiangzhan Co (Co = lake) in the west to Dingqing County in the east, with primarily Jurassic sandstone and limestone (Shi et al., 2006). Distinct glacial landforms formed by multiple glaciations are preserved throughout the whole range. These landforms have been investigated since the 1970s (Zhang, 1981; Li et al., 1986), with initial age constraints provided by lichenometry (Li et al., 1986), ^{14}C ages (Deng and Zhang, 1992; Li and Li, 1992; Jiao and Iwata, 1993) and other methods (Wang et al., 2007). In the past two decades, TCN dating techniques have been used to constrain ages of glacial landforms at the Tanggula Pass (Schäfer et al., 2002; Owen et al., 2005; Colgan et al., 2006) which is easily accessible by road. However, no progress had been made in the remote westernmost segment of this range. To address this gap and to enhance understanding of Quaternary glaciations and palaeoclimate and palaeoenvironment in the central TP an expedition was launched in 2019 to investigate glacial landforms on the eastern slope of Mount Geladandong. Historical records (topographical maps), high-resolution remote-sensing and GoogleEarth imagery, field mapping, and ^{10}Be surface exposure dating techniques were used to provide a preliminary new chronological framework of glacial fluctuations in this key area. In addition, we sampled erratics and an associated polished and striated bedrock surface to evaluate glacial erosion and nuclide inheritance, and we sampled the modern moraine complex to evaluate the upper limit of this dating techniques in a high-altitude area with a high ^{10}Be production rate.

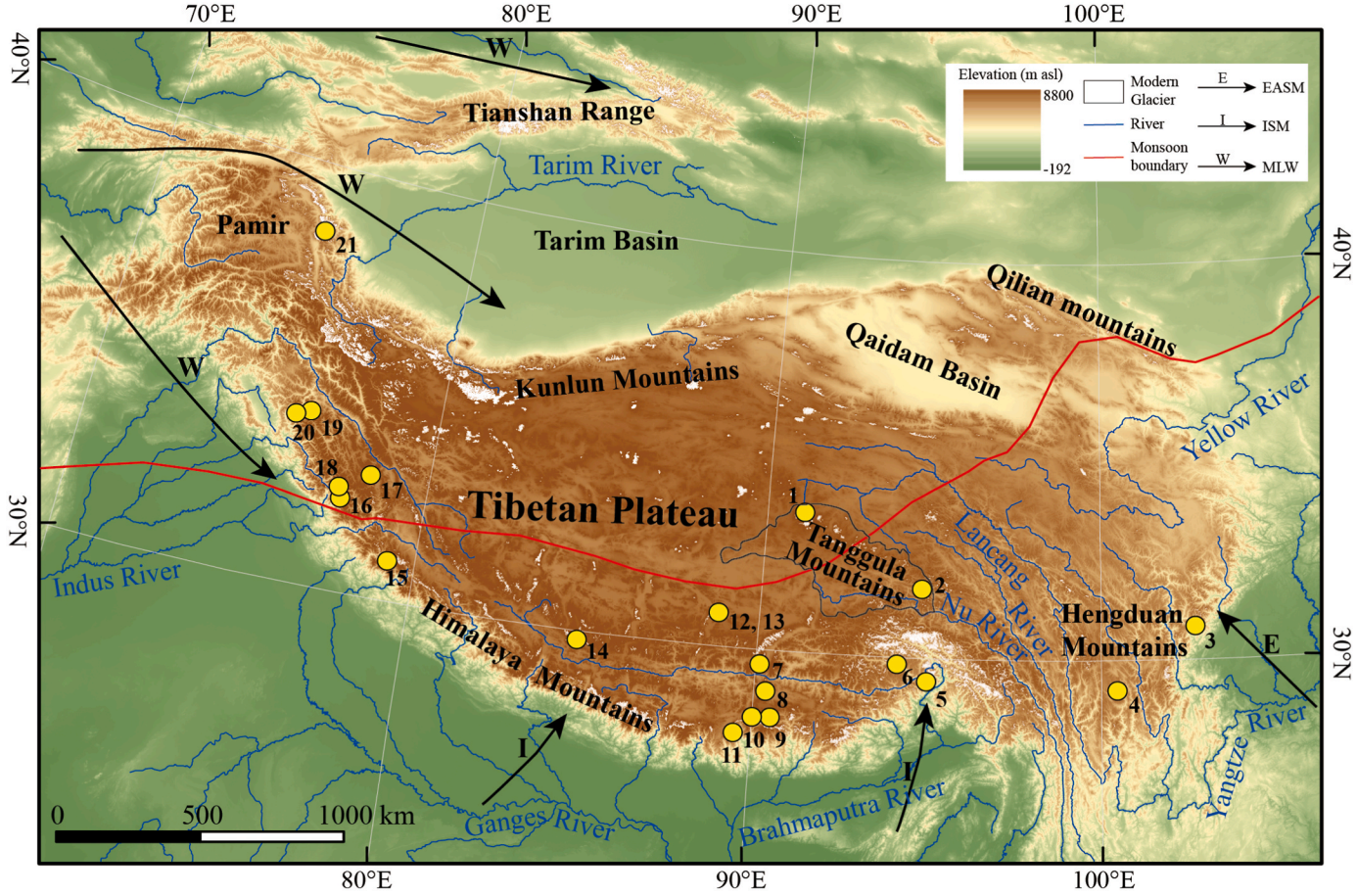

Fig. 1. Relief map of the Tibetan Plateau and its surrounding mountains including locations of ^{10}Be dating studies referred to in this paper.
1, Geladandong area, central TP; 2, Bujia Gangri, easternmost Tanggula Mountains (Zhao et al., 2023a,b); 3, Mt. Siguniang, Hengduan Mountains (Wang et al., 2023); 4, southern Shaluli Mountains (Chevalier and Replumaz, 2019); 5, Pai Valley, Mt. Namcha Barwa (Hu et al., 2020); 6, Basongcuo valley, near the eastern Himalayan syntaxis (Hu et al., 2017); 7, Quemuqu Valley, western Nyainqentanglha Mountains (Dong et al., 2017a); 8, Karola Pass, eastern Lhagoi Kangri Range (Liu et al., 2017); 9, Shimo Glacier Valley, Bhutanese Himalaya (Peng et al., 2020); 10, Cogarbu Valley, Bhutanese Himalaya (Peng et al., 2019); 11, Yadong rift, the Himalayas (Chevalier et al., 2022); 12, Mt. Jaggang, the Xainza range (Dong et al., 2017b); 13, eastern slope of Mount Jaggang, the Xainza range (Dong et al., 2018); 14, Gaerqiong Valley, central Gangdise Mountains (Zhang et al., 2018); 15, Central Garhwal, the western Himalayas (Murari et al., 2014); 16, Hamtah Valley, the western Himalayas (Saha et al., 2018); 17, Karzok Valley, the western Himalayas (Saha et al., 2018); 18, Kulti Valley, the western Himalayas (Saha et al., 2019); 19, Tarangoz Glacier Valley, Nun-Kun massif, northwestern India (Lee et al., 2014); 20, Parkachik Valley, Nun-Kun massif, northwestern India (Saha et al., 2019); 21, Muztag Ata and Kongur Shan, Eeatern Pamir (Seong et al., 2009). EASM: East Asian Summer Monsoon; ISM: Indian Summer Monsoon; MLW: middle-latitude westerlies. (Detailed information is provided in the supplementary materials (SM)).

2. Regional setting

The Tanggula Mountains act as important hydrologic and climatic boundaryies on the TP (Fig. 1). The Yangtze River and the Nu River originate from this range and flow into the Pacific Ocean and the India Ocean, respectively. In addition to providing exorheic drainage to the oceans, about one fifth of the drainage from the west segment of this range is endorheic, flowing into internal drainage basins on the TP (Li et al., 1986). Climatically, the Tanggula Mountains are influenced by the Indian and East Asian monsoons in summer and mid-latitude westerlies in winter (Chen et al., 2019). Annual precipitation is about 600~700 mm in the eastern part of the range and decreases to half this amount in the west, associated with east to west movement of the Indian Summer Monsoon along the southern side of the Tanggula Mountains (Li et al., 1986). Based on meteorological observations, the annual temperature at modern equilibrium-line altitude (ELA) in the Tanggula Mountains is estimated to be −6.0~-7.0 °C in the east, −8.0~-9.5 °C in the central region, and −10.4~-11.4 °C in the west (Shi et al., 2006).

The western segment of the Tanggula Mountains includes an extensive, well-preserved Tertiary planation surface with an altitude of ~6000 m. Its highest peak, Mt. Geladandong (6621 m asl), is the largest modern center of glaciation in the Tanggula Mountains. The precipitation and temperature regime and the characteristics of the modern glaciers indicate that they are typical continental type glaciers (Li et al., 1986), and the area includes cirque, valley, hanging and compound types of valley glaciers. The Second Glacier Inventory of China recorded

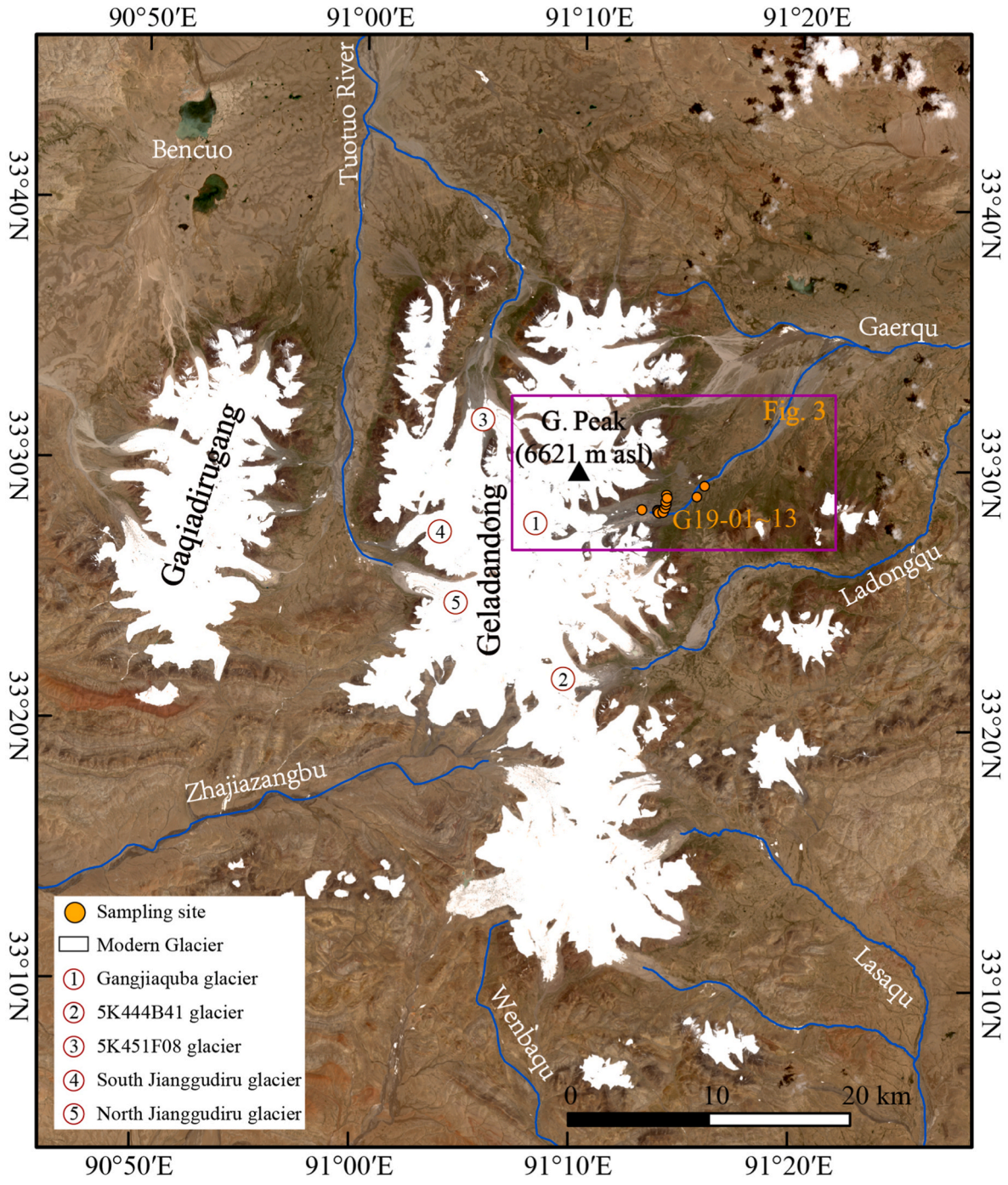

Fig. 2. Modern glacier distribution in the Geladandong area and ^{10}Be sampling sites.

219 modern active glaciers with an area of 845.17 km^2 and ice volume 81.1189 km^3 in the Geladandong area in 2007 (Guo et al., 2015; Liu et al., 2015), compared to 200 glaciers with a total area of 899.59 km^2 and an ice volume of 101.2226 km^3 in 1969 (Jiao and Zhang, 1988; Pu, 1994).

Five distinct compound valley glaciers are present around Mt. Geladandong, each with an area more than 30 km^2. They are the Gangjiaquba and No. 5K444B41 glaciers on the eastern slope, and No. 5K451F08, and the South and North Jianggudieru glaciers on the western slope (Fig. 2). The ablation areas of these compound valley glaciers are almost totally debris free, which is typical of modern glacier surfaces in the central TP, and contrasts with debris-laden glaciers that are typical of the Karakoram, Himalaya and Hengduan Mountains. The Gangjiaquba Glacier has a terminus at 5350 m asl, ~500 m below its ELA (5830 m asl), and only sporadic boulders are found on its ablation area.

3. Glacial landform mapping

Glacial landforms beyond the terminus of the Gangjiaquba Glacier were initially mapped based on topographical maps and high-resolution remote-sensing imagery. Morphological features, weathering conditions of moraines, and soil and vegetation development were investigated in the field and provide a relative age framework for these landforms (Figs. 2 and 3). The stratigraphical approach introduced by Hughes et al. (2005) to separate glacial landforms and successions in mountainous areas was adopted here. Based on the characteristics of moraine complexes, five sets of moraines were identified and numbered M_{E1} to M_{E5} from innermost (youngest) to outermost (oldest).

M_{E1} to M_{E3} moraine complexes occur in a flat U-shaped valley (Fig. 3). The M_{E1} moraine complex occurs within 4 km beyond the terminus of the Gangjiaquba Glacier. A comparison of historical records (topographical maps) and high-resolution remote-sensing imagery (Sentinel-2A, 2019-07-24), led to the M_{E1} moraine complex being divided into two sub-complexes (M_{E1-1} and M_{E1-2}). The inner M_{E1-1} moraine sub-complex was formed after 1969, indicating that the Gangjiaquba Glacier has retreated about 3.6 km during the past half century. The outer M_{E1-2} moraine sub-complex, which extends along ~0.5 km of the valley length was deposited before 1969. The M_{E1} moraine complex has no obvious sharp-crested frontal and lateral moraines and includes large angular and subangular boulders with fresh striations or polished surfaces. Based on observations of other moraines in the TP and its surroundings (Shi et al., 2006, 2011; Zhao et al., 2011), these characteristics suggest a fast retreat of the Gangjiaquba Glacier during the period since the Little Ice Age (LIA). Roche moutonnées, polished bedrock, and other features are also found in this part of the glacial valley.

The M_{E2} moraine complex occurs about 4.5 km beyond the terminus of the Gangjiaquba Glacier. Morphological and stratigraphic evidence indicates multiple glacial oscillation are recorded in this complex. Several end moraines with heights of about 3–5 m can be distinguished and these include boulders with striations or polished surfaces on them. Some of the boulders have been colonized by moss and lichen, and sparse grasses occur on the end moraines, however no soil has developed.

The M_{E3} moraine complex is about 6.2 km beyond the terminus of the Gangjiaquba Glacier, between 5300 m and 5150 m asl. The complex has undulating relief with alternating convex and concave topography

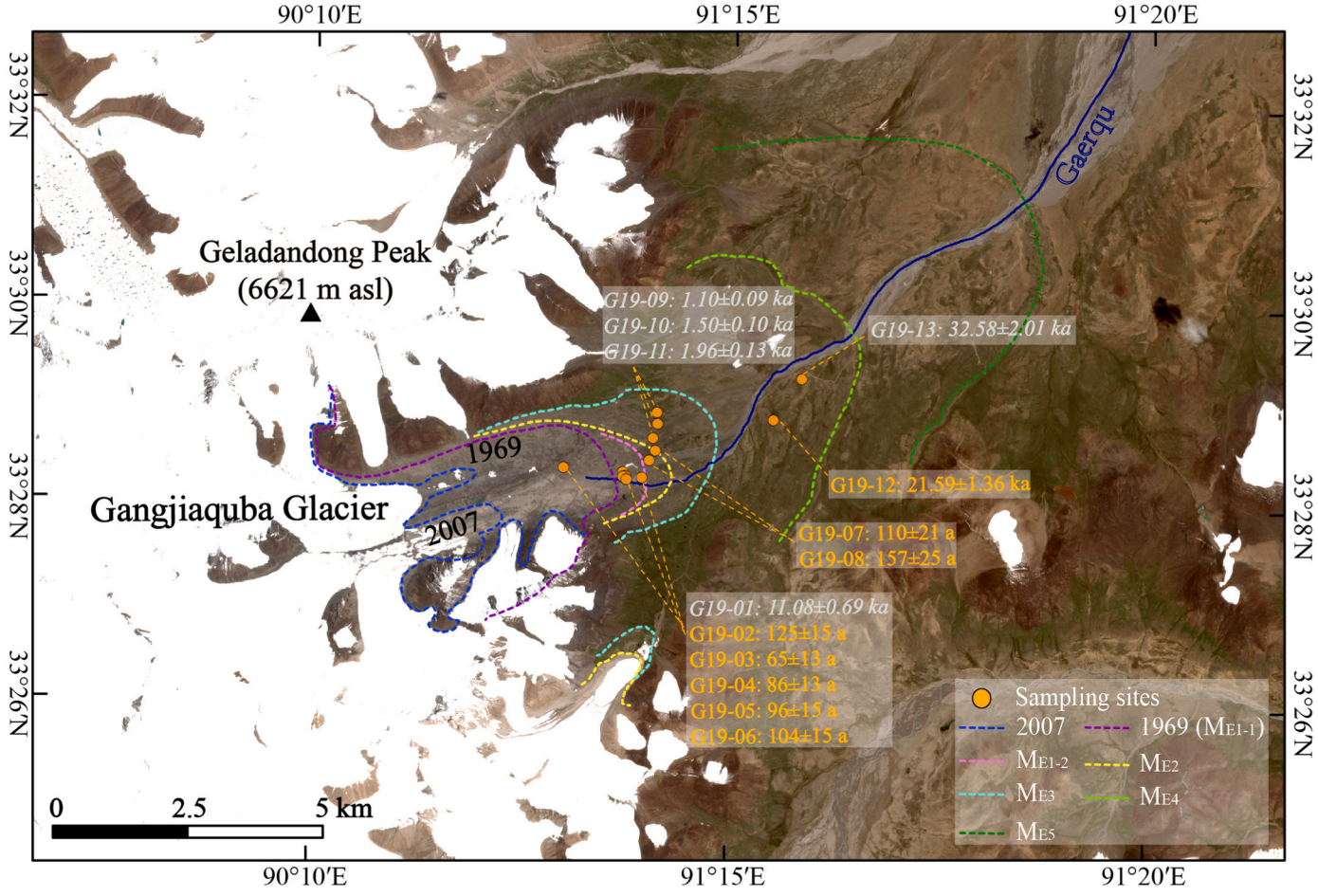

Fig. 3. Moraine complexes and their ^{10}Be ages (The sample numbers in gray italics are outliers that are also discussed in the text).

typical of hummocky moraine. It includes depressions 10–15 m in diameter and 3–5 m deep. A thin soil has developed on this moraine complex which supports sparse grass cover. The boulders show incipient weathering, and some are covered by moss and lichen. Meltwater erosion has cut a section through the moraine complex showing that the exposed till is about 5 m thick, and subrounded and subangular granite boulders typically 10–30 cm in diameter could be observed in the exposed section.

The position and landforms of the M_{E4} and M_{E5} moraine complexes indicate that large, dendritic compound valley glaciers developed here, with several tributary glaciers (Fig. 3). The M_{E4} moraine complex about 8.5 km from the current terminus of the Gangjiaquba Glacier, and much of the moraine complex has been eroded by meltwater and part has been covered by fluvial fans, especially in its northeastern area. The southern part of the M_{E4} moraine complex is about 20–30 m above the current stream, and the main remnant is a lateral moraine. A 10–15 cm thick gray-cinnamon soil has developed on M_{E4} moraines and supports alpine meadow vegetation. Sporadic large, weathered boulders protrude from this moraine complex.

In map view, the M_{E5} moraine complex is a relatively integrated arc (Fig. 3). The landform is a low gradient plain with half-buried granitic boulders 0.2–0.5 m in diameter on its surface. The boulders have been deeply weathered and have exfoliation fragments scattered around them. The weathering condition and characteristics of the moraine complex indicate that this landform was formed during an older glaciation than M_{E4}.

The lithologies of these glacial complexes are similar. The till clasts are mainly granite, sandstone, and limestone, with a small percentage of gneiss and conglomerate.

4. Cosmogenic nuclide methods

4.1. Sampling

The distribution and characteristics of M_{E1} moraine complex and a comparison of historical records (topographical maps) and high-resolution remote-sensing imagery indicate that the Gangjiaquba Glacier experienced dramatic retreats during the past century (Fig. 3). In order to evaluate nuclide inheritance and the upper limit of ^{10}Be surface exposure dating in this high-altitude area, six modern rock samples were collected from the M_{E1} moraine complex. Among them, one was derived from a quartz vein on bedrock and the other five ones were chiseled from the top surface layer of granitic boulders that deposited on the U-shaped valley bottom. We used a stratigraphical approach (Hughes et al., 2005) to guide our strategy in collecting seven samples from the M_{E2} to M_{E4} moraine complexes with the goal of establishing the moraine chronology.

We preferentially sampled the largest boulders that were stable on the trough bottom or embedded firmly in the moraine crests with obvious polished surfaces (Heyman et al., 2011). In addition, considering tall boulders more often yield well-clustered higher quality exposure ages than short boulders or groups including short boulders (Heyman et al., 2016), boulders less than 50 cm in height were avoided. The sampling location (latitude, longitude, and altitude) was recorded using a handheld global positioning system (GPS) instrument. The thickness of the sample taken, and the size of the boulder (length, width, and height) were measured. To determine shielding, detailed geomorphic context was measured using an inclinometer with 5° interval in both azimuth and elevation angles. Each boulder sampled was photographed from different directions (Fig. 4). Detailed information is given in Table 1 and all sampling pictures are given in supplementary materials (SM).

4.2. Sample preparation, measurement, and age calculation

Dating targets were prepared in the TCN Preparation Laboratory of SKLCS, Northwest Institute of Eco-Environment and Resources, CAS in Lanzhou, China. Quartz grains were extracted using the experimental procedure of Zhao et al. (2021), which was modified from Kohl and Nishiizumi (1992). Briefly, all rock samples were crushed and sieved, and fractions 250–500 μm in diameter were selected. H_2O_2 and HCl solutions were used to remove organic matter, carbonates, and other minerals. Magnetic and paramagnetic minerals were removed by Frantz magnetic separator (LB-1) with different currents. After the fractions were treated with 5% HF/HNO_3 solution twice, and each for 24 h with heating, a heavy-liquid (silicotungstic acid solution) was used to remove heavy and light acid-resistant minerals. Then, the fractions were leached two or three times with 1–2% HF/HNO_3 solution for 24 h with heating. Finally, the Al content in the quartz grains were checked by Inductively Coupled Plasma– Optical Emission Spectroscopy (ICP–OES).

The purified quartz grains with Al content less than 200 ppm were dissolved in concentrated HF solution with a spike of ^{9}Be carrier of about

Fig. 4. Representative photographs of glacially polished surfaces and boulders sampled for ^{10}Be surface exposure age dating.

Table 1
Sampling information for sites on the eastern slope of Mount Geladandong, westernmost Tanggula Mountains, central Tibetan Plateau.

Glacial stage	Sample ID	Latitude (°N)	Longitude (°E)	Elevation (m asl)	Boulder size L/W/H (cm)	Thickness (cm)	Topographic shielding factor
M_{E1-1}	G19-01	33.47265	91.21555	5327	bedrock	2.3	0.96557
M_{E1-2}	G19-02	33.47210	91.22753	5291	355/190/57	2.0	0.97003
	G19-03	33.47148	91.22801	5296	368/292/200	3.0	0.96691
	G19-04	33.47143	91.22756	5291	190/188/115	2.0	0.96214
	G19-05	33.47096	91.22825	5300	160/120/120	2.0	0.98029
	G19-06	33.47113	91.23130	5287	283/235/190	2.5	0.97984
M_{E2}	G19-07	33.47408	91.23270	5285	250/166/120	2.5	0.97963
	G19-08	33.47566	91.23386	5290	256/170/95	2.0	0.98187
M_{E3}	G19-09	33.47776	91.23345	5294	110/95/70	2.8	0.98229
	G19-10	33.48208	91.23414	5296	200/155/140	2.0	0.98592
	G19-11	33.48018	91.23428	5293	140/95/70	3.0	0.98606
M_{E4}	G19-12	33.48111	91.25742	5242	200/110/80	2.8	0.98569
	G19-13	33.48798	91.26295	5224	230/220/75	1.9	0.98724

0.27 g with a concentration of 982.3 ppm. Then, fluoride compounds removed by fuming with $HClO_4$, Be was isolated using standard anion and cation exchange chromatography procedures, NH_4OH was added and $Be(OH)_2$ was precipitated with pH value at about 8.5. Finally, the Be $(OH)_2$ was placed in a quartz crucible and decomposed to BeO at 950 °C in a muffle furnace. A mixture of the BeO and niobium powder was loaded into steel cathodes for accelerator mass spectrometry (AMS) analysis.

The $^{10}Be/^{9}Be$ ratios were measured by AMS at the Purdue Rare Isotope Measurement Laboratory (PRIME Lab), Purdue University, with normalization of the revised ICN standard (07KNSTD, Nishiizumi et al., 2007). The measured $^{10}Be/^{9}Be$ ratios were corrected by the corresponding chemical procedural blanks and converted to ^{10}Be concentrations in quartz for final apparent exposure age calculation. Topographic shielding was calculated using field records and were also compared with results from the Python tool developed by Li (2018). Quartz weights, ^{9}Be carrier masses, $^{10}Be/^{9}Be$ ratios, and chemical process blanks are all listed in Table 2.

The CRONUS-Earth online calculator version 3 (http://hess.ess.washington.edu/math/v3/v3_age_in.html) (Balco et al., 2008) was used to calculate apparent ^{10}Be exposure ages. Rock density was set at 2.7 g/cm^3, the surface erosion was assumed to be zero, the potential impacts of snow cover were not considered. As a result of these assumptions, our ages should be considered as apparent minimum estimates. In Table 2, the ^{10}Be ages with three scaling schemes are listed, only the ages using the Lifton-Sato-Dunai (LSDn) scaling scheme (Lifton et al., 2014) are reported and discussed in the text. The ^{10}Be dates that we refer to for comparison to our results, mainly published since 2014, were recalculated using this online calculator too.

5. Cosmogenic nuclide results

For ^{10}Be surface exposure dating, an ideal scenario is that samples have not been exposed before they were deposited and have been exposed continuously since they were deposited. Prior exposure (nuclide inheritance) will result in overestimated ages, and incomplete exposure (such as moraine degradation, boulder toppling, exhumation, shielding, and weathering) will result in underestimated ages (Heyman et al., 2011). In this study, our dating results are generally consistent with the glacial sequence, their morphological positions, the degree of weathering and the characteristics of moraines (Figs. 2–4 and SM).

The moraine complexes and their ^{10}Be ages are shown in Fig. 3. Sample G19-01 is a quartz vein in bedrock within the area of the M_{E1-1} moraine complex that we know from historical data (topographical map) was exposed after 1969. Its apparent exposure age (11.08 ± 0.69 ka) suggests considerable inheritance. Samples G19-02∼06 collected on boulders from M_{E1-2} and were dated to 125 ± 15 a, 65 ± 13 a, 86 ± 13 a, 96 ± 15 a and 104 ± 15 a respectively. These ages are generally consistent with the characteristics of this fresh moraine sub-complex and the historical data. Samples G19-07 and G19-08 were derived from the innermost end moraine of M_{E2}, and give ages of 110 ± 21 a and 157 ± 25 a. Samples G19-09∼11 from M_{E3} give ^{10}Be ages of 1.10 ± 0.10 ka, 1.50 ± 0.10 ka and 2.00 ± 0.13 ka respectively. Samples G19-12 and G19-13 from M_{E4} were dated to 21.59 ± 1.36 ka and 32.58 ± 2.01 ka. Except for the age of bedrock, the dates of boulders show a progression from young to old, consistent with the glacial successions and their geomorphological relationships. However, considering the characteristics of the M_{E3} moraine complex and two inconsistent ages in the M_{E4} moraine complex, it is important to be cautious in assigning a definitive age or a glacial event to these two moraine complexes.

6. Discussion

The glacial landforms on the eastern slope of Mount Geladandong provide a promising opportunity to establish a preliminary chronological framework for glacial events in the westernmost segment of the Tanggula Mountains, central TP. The ^{10}Be dating results, especially the ages of M_{E1} moraine complex also give us a chance to evaluate subglacial erosion, potential prior exposure (nuclide inheritance) of young boulders and to discuss the upper limit of the ^{10}Be exposure dating techniques. The inconsistent three ages of M_{E3} moraine complex are used to discuss the surface instability of hummocky moraines.

Topographical map data and high-resolution remote-sensing imagery show that site G19-01 was covered by the glacier before 1969 (Fig. 3). Thus, the most recent exposure age of this glacially-polished surface should be only tens of years, compared to an apparent exposure age of 11.08 ± 0.69 ka. Previous studies have shown that the ages or nuclide concentrations for glacially-polished surfaces can be greater than those of nearby glacially transported boulders (Briner and Swanson, 1998; Bierman et al., 1999), whereas in other situations the ages of the glacially-polished surfaces are consistent with their geological settings (Nishiizumi et al., 1989; Clark et al., 1995; Kelly et al., 2006; Zhang et al., 2016). In cases where the glacially polished surfaces have apparent exposure ages that are older than those of glacially transported boulders on the same surface, it is inferred that glacial erosion was insufficient (<2 m) to remove prior inheritance. Based on the variation of TCN concentration with depth in a rock surface (Gosse and Phillips, 2001), the differences in ages can in some cases be used to infer depths of prior glacial erosion (e.g., Fabel et al., 2002, 2004; Li et al., 2005). The striations on the bedrock surface at G19-01 demonstrate that the sampling site has been eroded, however the age of 11.08 ± 0.69 ka on this site we know was exposed most recently within the past 50 years indicates that the erosion under the most recent period of glaciation was insufficient (<2 m) to remove inheritance. One possible reason for small amounts of subglacial erosion is that the Gangjiaquba Glacier may have been cold-based part time. The fact that the surface, even after some erosion, has a ^{10}Be concentration equivalent to 11ka of exposure indicates that it had a long period of exposure prior to the global Last Glacial Maximum (LGM_G).

Based on geomorphological position and characteristics, the M_{E1-2}

Table 2
^{10}Be apparent exposure ages calculated using the CRONUS online calculator.

Sample ID	Quartz (g)[a]	^{9}Be carrier (g)	^{10}Be/^{9}Be (10^{-15})[b]	^{10}Be concentration (10^{3} atoms/g)	St[c]			Lm[d]			LSDn[e]		
					Age (years)	Internal error (years)	External error (years)	Age (years)	Internal error (years)	External error (years)	Age (years)	Internal error (years)	External error (years)
G19-01	40.0031	0.2717	2038.8003 ± 32.5115	908.060 ± 17.113	10,305	195	839	11,165	211	866	11,076	209	688
G19-02	40.2032	0.2722	19.2187 ± 1.5397	7.583 ± 0.760	87	9	11	118	12	15	125	13	15
G19-03	41.2763	0.2713	11.2396 ± 1.6413	3.916 ± 0.775	45	9	10	60	12	13	65	13	13
G19-04	40.2001	0.2726	13.8288 ± 1.5119	5.197 ± 0.745	60	9	10	81	12	13	86	12	13
G19-05	40.1749	0.2738	15.3612 ± 1.6894	5.913 ± 0.824	67	9	11	90	13	14	96	13	15
G19-06	40.2951	0.2727	16.4492 ± 1.7104	6.351 ± 0.827	72	9	11	98	13	15	104	14	15
G19-blank1		0.2725	2.1542 ± 0.7182										
G19-07	40.1818	0.2750	20.9524 ± 1.7907	6.714 ± 1.224	76	14	15	104	19	20	110	20	21
G19-08	40.2915	0.2748	27.3724 ± 2.3034	9.564 ± 1.385	108	16	18	149	22	24	157	23	25
G19-09	40.0661	0.2746	196.4340 ± 10.8134	85.671 ± 5.030	971	57	96	1112	65	106	1100	65	92
G19-10	40.2045	0.2753	277.5890 ± 6.8686	122.081 ± 3.454	1368	39	115	1516	43	122	1497	42	98
G19-11	40.5902	0.2748	356.9660 ± 8.0515	155.973 ± 4.018	1765	45	147	1961	51	156	1958	50	126
G19-12	4.6517	0.2737	536.5761 ± 9.6889	2049.208 ± 43.508	23,810	509	1959	22,680	484	1778	21,585	461	1361
G19-13	40.3397	0.2752	7188.0697 ± 89.3056	3216.398 ± 51.348	37,446	603	3046	34,929	563	2702	32,580	524	2008
G19-blank2		0.2748	1.2123 ± 0.4583										

[a] The concentration of ^{9}Be carrier is 982.3 ppm.
[b] The ratio of^{10}Be/^{9}Be was measured in PRIME laboratory, Purdue University, with isotope ratios normalized to standard 07KNSTD (Nishiizumi et al., 2007).
[c] St represents time-independent production rate scaling scheme of Lal (1991)/Stone (2000).
[d] Lm represents time-dependent production rate scaling scheme of Lal (1991)/Stone (2000).
[e] LSDn represents time- and nuclide-dependent scaling scheme of Lifton et al. (2014).

moraine complex was inferred to have been deposited since the LIA but before 1969. Five dates, ranging from 65 ± 13a to 125 ± 15 a are consistent with these limits. The consistency of the dating results suggests that there is no or negligible nuclide inheritance in these samples, in other words, the boulders that have been sampled had not been exposed before they were deposited. These dating results demonstrate that ^{10}Be surface exposure dating techniques can used to investigate samples with only decades of exposure at high altitudes, because of the high ^{10}Be production rate in this environment.

Based on the glacial depositional sequence and characteristics of moraine complexes, sharp-crested fresh end moraines beyond the modern glacial landforms in the TP and its surroundings have been presumed to have formed during LIA period (Shi et al., 2006, 2011; Zhao et al., 2011). Based on the scope of the LIA defined by the IPCC (2013), these glacial advances should have occurred during cold periods since 15th century. Two ages (G19-07: 110 ± 21 a, and G19-08: 157 ± 25 a) from the innermost end moraine of M_{E2} indicate that this moraine complex was formed during the LIA. Recently, LIA glacial advances have been identified by ^{10}Be dating results in many regions in the TP and its surroundings, for example, two moraines on the eastern slope of Mount Jaggang, Xainza Range (Dong et al., 2017b); the latest moraine complexes in two valleys around the Karola Pass (Liu et al., 2017); two moraines in the Gaerqiong valley, central Gangdise Mountains (Zhang et al., 2018); a moraine complex in the Cogarbu valley and Shimo Glacier valley on the northern slope of the Bhutanese Himalaya (Peng et al., 2019, 2020); and the end moraines that act as lake dams on the southern slope of Bujia Gangri, eastern Tanggula Mountains (Zhao et al., 2023a,b). In the western Himalaya, contemporaneous glacial advances have also been investigated using ^{10}Be dating techniques (Lee et al., 2014; Murari et al., 2014; Saha et al., 2018, 2019). Consistent with the conclusions of several comprehensive review papers (Dortch et al., 2013; Murari et al., 2014; Owen and Dortch, 2014; Xu and Yi, 2014), LIA glacial advances have been identified in every major range that has been studied in the TP and its surroundings.

Many climate archives have been used to investigate climate during the LIA. δ^{18}O records from ice cores in the TP revealed that a cooling period occurred from AD ~1600–1870 (Thompson et al., 2006). A cold period corresponding to the LIA has been suggested by multiple proxies across the whole TP, including fossil pollen, leaf wax δD, ice core δ^{18}O, carbonate δ^{18}O, alkenones, glycerol dialkyl glycerol tetraethers (=GDGTs) and chironomids (Chen et al., 2020 and references therein). Net mass accumulation records of ice cores from the TP indicate higher precipitation occurred in the 17th and 18th centuries, and lower precipitation in the 19th century (Thompson et al., 2006). Whereas, in monsoonal Central Asia, a moderate dry period occurred during the Late Holocene (Herzschuh, 2006). It is clear that the spatial and temporal pattern of temperature and precipitation variation across the TP and surrounding regions is complex. A study in the Muztag Ata and Kongur Shan, in the eastern Pamir Plateau has found that palaeoglacier oscillations during the Late Glacial and Holocene were synchronous with ice-rafting events and autocyclicity in the North Atlantic (Seong et al., 2009), suggesting that the cooling signals in the North Atlantic could be transmitted to the TP by the mid-latitude westerly system. Subsequent studies on LIA glacial advances in the Himalayas (Rowan, 2017), and on the northern slope of the Bhutanese Himalaya, eastern Himalaya (Peng et al., 2019, 2020), suggested similar teleconnections. Therefore, it is possible to hypothesize that the LIA glacial advance in the Mount Geladandong area, central TP was driven by cooling signals from the North Atlantic area.

Three samples collected from the M_{E3} moraine complex were dated to 1.10 ± 0.10 ka (G19-09), 1.50 ± 0.10 ka (G19-10) and 2.00 ± 0.13 ka (G19-11) respectively, however, the scattered dating results make it difficult to assign an age or a specific glacial event to this landform. The characteristics of this moraine complex suggest that it is hummocky moraine. Previous studies have suggested that the instability of surface process could make the "real ages" of hummocky moraine older than the apparent oldest dating results (Zech et al., 2005; Reuther et al., 2011; Zech, 2012; Çiner et al., 2015; Zhao et al., 2023a,b). The discrepancy between dating results and the actual ages of hummocky moraines is caused by the melting of buried dead ice which produces long-lived surface instability. In early studies of the M_{E3} moraine complex its age was constrained by several indirect ^{14}C ages. The meadow soil that covers this moraine complex was dated to 3540 ± 160 a BP (Deng and Zhang, 1992); and the organic matter in soil that covers the outmost and innermost moraine were dated to 5410 ± 225 a BP and 2690 ± 110 a BP (Li and Li, 1992). Although there are no detailed descriptions of sections and ^{14}C dating methods, these indirect ^{14}C ages can also be used to constrain this moraine complex. In addition, a comprehensive study of climate change, vegetation history, and landscape responses during the Holocene across the whole TP indicated that glacial advances decreased during the mid-Holocene, and increased substantially after 3 ka (Chen et al., 2020). Considering the both the ^{14}C ages and the ^{10}Be apparent exposure ages, we tentatively assign M_{E3} to the period of Neoglaciation (glacial advances mainly occurring during 3–4 ka) rather than our oldest ^{10}Be age (2.00 ± 0.13 ka (G19-11)) which we consider to be a minimum limiting age for M_{E3}.

Previous studies have shown that glacial advances during the Neoglacial happened in many ranges in the TP and its surroundings (Shi et al., 2006, 2011; Zhao et al., 2011; Dortch et al., 2013; Murari et al., 2014; Owen and Dortch, 2014). This glacial event roughly corresponds to the regional glacial stage SWHTS 1C in the semi-arid western end of the Himalayan-Tibetan orogen (Dortch et al., 2013), and to the MOHITS 1E glacial stage in the monsoon-influenced Himalaya-Tibetan area (Murari et al., 2014). Based on decreasing monsoon influence, Dortch et al. (2013) suggested that the SWHTS 1C glacial stage could be tied to northern hemisphere oscillations with a dominant moisture supply brought via the mid-latitude westerlies. Considering the modern monsoon boundary (Fig. 1) (Chen et al., 2019), it is also reasonable for us to conclude that the glacial advance that formed the M_{E3} moraine complex had this forcing mechanism. However, more work needs to be done to better constrain the age of this moraine complex.

The apparent exposure age of G19-12 (21.59 ± 1.36 ka) from the M_{E4} moraine complex is within LGM_G as defined by the EPILOG research group (Mix et al., 2001) and Clark et al. (2009). This is corroborated by an indirect ^{14}C age (18,010 ± 386 a BP) for peat from a deposit outside a moraine that was identified as being formed at the same period as the M_{E4} moraine complex (Deng and Zhang, 1992). As noted previously, no detailed information is provided about these ^{14}C ages, which limits further evaluation of their significance.

The apparent ^{10}Be exposure age of G19-13 (32.58 ± 2.01 ka) is beyond the LGM_G range, and could support the moraine being assigned to late period of marine oxygen isotope stage (MIS) 3. There has been extensive discussion in the literature about whether there is compelling evidence for MIS 3 advances across the TP and adjacent mountain ranges (Schaefer et al., 2008; Owen and Dortch, 2014 and references therein). This includes from research at the Tanggula Pass (Jiao and Iwata, 1993; Colgan et al., 2006) and a recent study in the easternmost segment of this range (Zhao et al., 2023a), as well as implications of a relatively warm climate revealed by the δ^{18}O records in the Guliya ice core during the late MIS 3 (Shi et al., 2001). Given other apparent exposure ages and the ^{14}C age data, we initially conclude that the M_{E4} moraine complex was formed during LGM_G glacial event and that G19-13 has ^{10}Be inheritance. However, sampling additional boulders in the M_{E4} moraine complex should be a priority to provide additional evidence for its age.

Geological evidence of palaeoglacier advances during the LGM_G have been identified in almost every range in the TP and its surroundings (Shi et al., 2006, 2011; Dortch et al., 2013; Murari et al., 2014; Owen and Dortch, 2014). In the past decade, LGM_G glacial events have been identified by ^{10}Be surface exposure dating techniques in the Gangbu Valley in the Lhagoi Kangri Range, the Himalayas (Liu et al., 2017), in the Quemuqu valley in the western Nyainqentanglha mountains (Dong et al., 2017a), in the Xainza range, central Tibet (Dong et al., 2018), in

the Cogarbu valley on the northern slope of the Bhutanese Himalaya (Peng et al., 2019), in the southern Shaluli Mountains (Chevalier and Replumaz, 2019), and in the southern Yadong rift in southern Tibet (Chevalier et al., 2022), in the Changping Valley on the southwestern slope of Mount Siguniang, Hengduan Mountains (Wang et al., 2023). In addition, an outermost latero-frontal moraine of the most extensive paleoglacial event in the Basongcuo catchment, near the eastern Himalayan syntaxis (Hu et al., 2017), and the M3 moraine in the Pai Valley alongside Namcha Barwa (Hu et al., 2020) were constrained to the LGM_G by ^{10}Be and OSL dating results.

Palaeoclimate proxies in the TP and its surroundings have been used to investigate possible climate forcing mechanisms for the LGM_G glaciation. The LGM_G period is in phase with the Guliya ice core negative $\delta^{18}O$ excursion (Thompson et al., 1997) throughout MIS 2 (Fig. 5), and it is also in phase with the speleothem negative $\delta^{18}O$ excursion in East Asia Monsoon area (Wang et al., 2008). In addition, this timeframe also corresponds with the largest peak of the global ice volume during the last glacial cycle (Lisiecki and Raymo, 2005) and low insolation at 65° in the Northern Hemisphere (Berger and Loutre, 1991). Based on multiple climate proxies, a comprehensive study of palaeoglaciers and their environmental variations on the Tibetan Plateau showed that the temperature during LGM_G is about 7 °C lower than present, meanwhile, the precipitation is only 30–70% of present-day levels (Shi et al., 1997). Thus, we infer that the M_{E4} moraine complex formed during LGM_G was a response to a temperature reduction rather than a precipitation increase.

The outline of the M_{E5} moraine complex is very clear on remote sensing images (Fig. 3). Its characteristics, including low gradient terrain, and half-buried granitic boulders with extensive weathering, indicate that this landform formed during an older glaciation than M_{E4}. After this glaciation, the landform underwent much erosion and the landscape during this glaciation would have been quite different from the present style. Therefore, more work needs to be done before it can be assigned to a specific glacial event or age.

Palaeo-ELAs and their changes (ΔELAs) are important climatic indicators, and they can be used to assess the combinations of temperature and precipitation changes that occurred during past periods. There are several methods to reconstruct palaeo-ELAs (Benn and Lehmkuhl, 2000; Porter, 2001). Here we use the modern ELA (5820 m asl) and an accumulation area ratio (AAR) of 0.65 with limits of past glacial extent to reconstruct and discuss palaeo-ELAs and evaluate ΔELAs during the LIA and other periods (Table 3). The reconstructed ELAs of 1969, LIA, Neoglacial, LGM_G and pre-LGM_G were 5710 m, 5682 m, 5596 m, 5508 m and 5483 m, respectively, and ΔELAs were 110 m, 138 m, 224 m, 312 m and 437 m respectively. These results for palaeo-ELAs and ΔELAs are consistent with previous studies by Li et al. (1991) and Shi et al. (2006). Our results further confirm the conclusion that the decrease of ELAs during glacial events in the central TP are less than in surrounding areas, linked to a cold and dry climate during glacial periods in the central TP.

7. Conclusions

^{10}Be ages, historical records, and geomorphological relationships help us to identify multiple glacial events on the eastern slope of Mount Geladandong, central TP. The $M_{E1\text{-}1}$ and $M_{E1\text{-}2}$ moraine complexes were formed in the past century, since the LIA, and the M_{E2} moraine complex was deposited during the LIA glacial advance. The M_{E3} and M_{E4} moraine complexes were tentatively assigned to the Neoglaciation and LGM_G glacial events. The M_{E5} moraine complex was formed during a pre-LGM_G glaciation. The reconstructed palaeo-ELAs and their decreases further confirm that ELA decreases during glacial events in the central TP are less than those in surrounding areas.

The ^{10}Be ages of boulders from the youngest glacial complex (M_{E1}) demonstrate that there are no or negligible nuclide inheritance for the boulders that were sampled and, based on correspondence with the

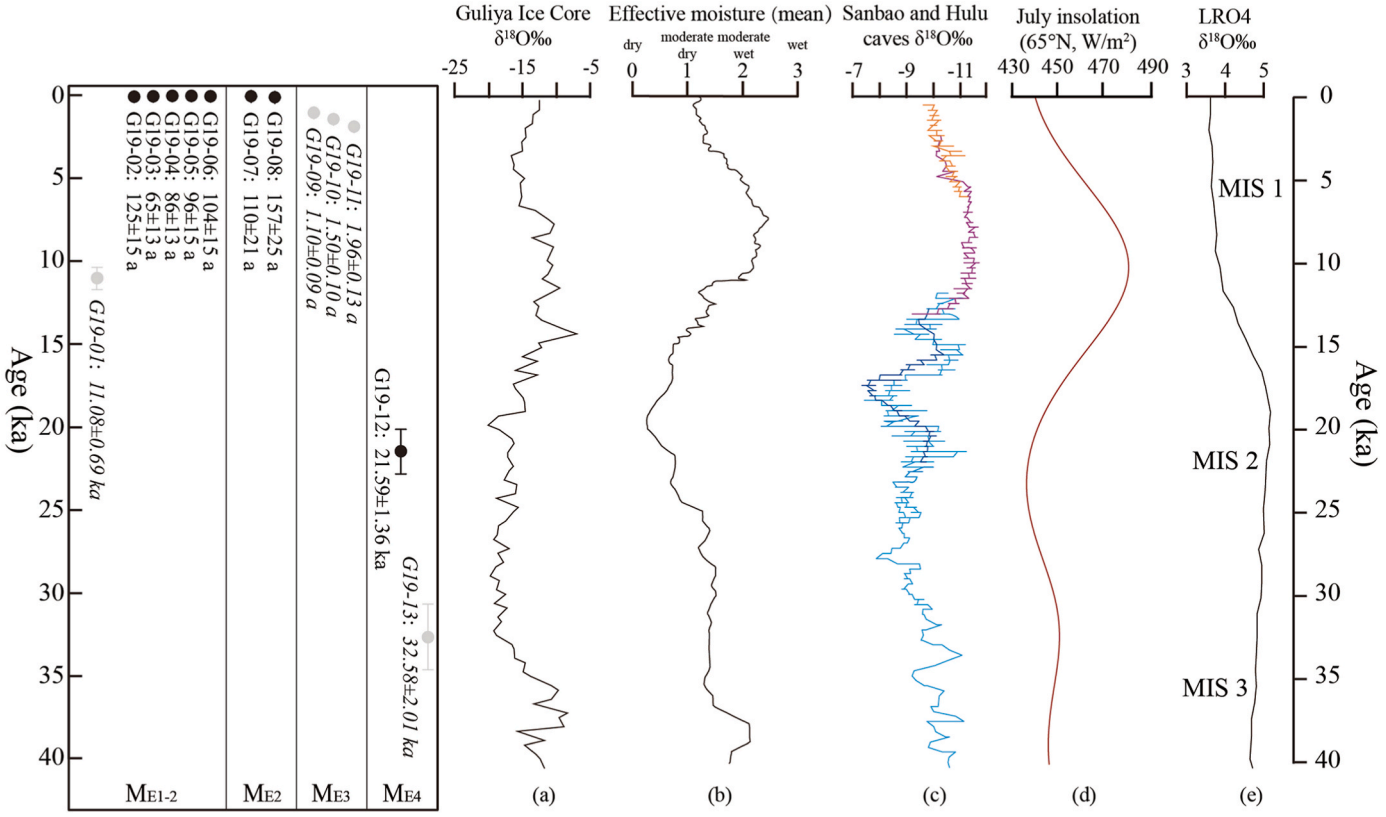

Fig. 5. A comparison of our ^{10}Be ages with other climate proxies: a, $\delta^{18}O$ records of the Guliya ice core (Thompson et al., 1997); b, mean effective moisture in monsoonal Central Asia (Herzschuh, 2006); c, $\delta^{18}O$ records from the Sanbao and Hulu caves (Wang et al., 2008); d, July insolation at 65°N (Berger and Loutre, 1991); e, $\delta^{18}O$ records for LR04 (Lisiecki and Raymo, 2005).

Table 3
Parameters, ELAs and their decrease for the reconstructed Gangjiaquba Glacier in 1969, during the LIA, Neoglacial, LGM_G and pre-LGM_G.

	Summit (m asl)	Terminus (m asl)	Length (km)	Coverage (km^2)	ELA (m asl)	ΔELA (m)
Contemporary	6621	5415	7.46	28.86	5820	N/A
1969	6621	5300	10.6	37.44	5710	110
LIA	6621	5272	11.65	46.92	5682	138
Neoglacial	6621	5235	13.38	69.13	5596	224
LGM_G	6621	5192	15.82	93.00	5508	312
pre-LGM_G	6621	5127	19.83	124.62	5483	437

historical record indicate that ^{10}Be surface exposure dating techniques can be used to investigate glacial landforms that have only tens of years of exposure at high altitudes, because of the high ^{10}Be production rate at this elevation. The data presented here also suggests that a cautious sampling and interpretation strategy should be adopted with bedrock samples, because of potential inheritance due to limited subglacial erosion, and that ^{10}Be ages of hummocky moraines need a cautious explanation when there a high level of scatter in the ages.

Author contributions

J.D. Zhao designed and conducted the fieldwork, experiments; J.K. Qiu conducted the experiments and ages calculation; J.D. Zhao, J.M. Harbor and M.W. Caffee conducted ^{10}Be data analysis and interpretation; W.Q. Guo and H.H. Ji prepared the figures; X.B. He conducted the fieldwork and provided logistics supports. All authors contributed to writing, reviewing, and editing the paper.

Data availability

Data from this study are available on request (jdzhao@lzb.ac.cn).

Declaration of competing interest

The authors declare that they have no known competing financial interests or personal relationships that could have appeared to influence the work reported in this paper.

Acknowledgements

We thank Ruilian Liu, Yuming Lu and Linwei Lu for their fieldwork assistance. We thank Thomas E. Woodruff for helping measure the ^{10}Be dating targets in the PRIME Laboratory. This work was supported by the National Natural Science Foundation of China (Nos. 41830644; 41771018; 42271156), the Second Tibetan Plateau Scientific Expedition and Research Program (No. 2019QZKK0201), the Science and Technology Program of Tibet (XZ202301ZY0001G), and the PRIME Laboratory seed program. Harbor's work was supported by Purdue University Global.

Appendix A. Supplementary data

Supplementary data to this article can be found online at https://doi.org/10.1016/j.quaint.2023.12.004.

References

Balco, G., 2020. Glacier change and paleoclimate applications of cosmogenic-nuclide exposure dating. Annu. Rev. Earth Planet Sci. 48, 21–48.
Balco, G., Stone, J.O., Lifton, N.A., Dunai, T.J., 2008. A complete and easily accessible means of calculating surface exposure ages or erosion rates from ^{10}Be and ^{26}Al measurements. Quat. Geochronol. 3, 174–195.
Benn, D.I., Lehmkuhl, F., 2000. Mass balance and equilibrium-line altitudes of glaciers in high-mountain environments. Quat. Int. 65 (66), 15–29.
Berger, A., Loutre, M.F., 1991. Insolation values for the climate of the last 10 million years. Quat. Sci. Rev. 10, 297–317.
Bierman, P.R., Marsella, K.A., Patterson, C., Davis, P.T., Caffee, M., 1999. Mid-Pleistocene cosmogenic minimum-age limits for pre-Wisconsinan glacial surfaces in southwestern Minnesota and southern Baffin Island: a multiple nuclide approach. Geomorphology 27, 25–39.
Briner, J.P., Swanson, T.W., 1998. Using inherited cosmogenic ^{36}Cl to constrain glacial erosion rates of the Cordilleran ice sheet. Geology 26, 3–6.
Chen, F.H., Chen, J.H., Huang, W., Chen, S.Q., Huang, X.Z., Jin, L.Y., Jia, J., Zhang, X.J., An, C.B., Zhang, J.W., Zhao, Y., Yu, Z.C., Zhang, R.H., Liu, J.B., Zhou, A.F., Feng, S., 2019. Westerlies Asia and monsoonal Asia: spatiotemporal differences in climate change and possible mechanisms on decadal to sub-orbital timescales. Earth Sci. Rev. 192, 337–354.
Chen, F.H., Zhang, J.F., Liu, J.B., Cao, X.Y., Hou, J.Z., Zhu, L.P., Xu, X.K., Liu, X.J., Wang, M.D., Wu, D., Huang, L.X., Zeng, T., Zhang, S., Huang, W., Zhang, X., Yang, K., 2020. Climate change, vegetation history, and landscape responses on the Tibetan Plateau during the Holocene: a comprehensive review. Quat. Sci. Rev. 243, 106444.
Chevalier, M.L., Replumaz, A., 2019. Deciphering old moraine age distributions in SE Tibet showing bimodal climatic signal for glaciations: marine Isotope Stages 2 and 6. Earth Planet Sci. Lett. 507, 105–118.
Chevalier, M.L., Replumaz, A., Wang, S.J., Pan, J.W., Bai, M.K., Li, K.Y., Li, H.B., 2022. Limit of monsoonal precipitation in southern Tibet during the Last Glacial Maximum from relative moraine extents. Geomorphology 397, 108012.
Çiner, A., Sarıkaya, M.A., Yıldırım, C., 2015. Late Pleistocene piedmont glaciations in the Eastern Mediterranean; insights from cosmogenic ^{36}Cl dating of hummocky moraines in southern Turkey. Quat. Sci. Rev. 116, 44–56.
Clark, D.H., Bierman, P.R., Larsen, P., 1995. Improving in situ cosmogenic chronometers. Quat. Res. 44, 367–377.
Clark, P.U., Dyke, A.S., Shakun, J.D., Carlson, A.E., Clark, J., Wohlfarth, B., Mitrovica, J. X., Hostetler, S.W., McCabe, A.M., 2009. The last glacial maximum. Science 325, 710–714.
Colgan, P.M., Munroe, J.S., Zhou, S.Z., 2006. Cosmogenic radionuclide evidence for the limited extent of last glacial maximum glaciers in the Tanggula Shan of the central Tibetan Plateau. Quat. Res. 65, 336–339.
Deng, X.F., Zhang, W.J., 1992. Evolution of Quaternary glaciers and environment on the eastern side of the Geladandong Peak (in Chinese with English abstract). J. Glaciol. Geocryol. 14, 153–160.
Dong, G.C., Xu, X.K., Zhou, W.J., Fu, Y.C., Zhang, L., Li, M., 2017a. Cosmogenic ^{10}Be surface exposure dating and glacier reconstruction for the last glacial maximum in the Quemuqu Valley, western Nyainqentanglha mountains, south Tibet. J. Quat. Sci. 32, 639–652.
Dong, G.C., Zhou, W.J., Yi, C.L., Fu, Y.C., Zhang, L., Li, M., 2018. The timing and cause of glacial activity during the last glacial in central Tibet based on ^{10}Be surface exposure dating east of Mount Jaggang, the Xainza range. Quat. Sci. Rev. 186, 284–297.
Dong, G.C., Zhou, W.J., Yi, C.L., Zhang, L., Li, M., Fu, Y.C., Zhang, Q., 2017b. Cosmogenic ^{10}Be surface exposure dating of 'Little Ice Age' glacial events in the Mount Jaggang area, central Tibet. Holocene 27, 1516–1525.
Dortch, J.M., Owen, L.A., Caffee, M.W., 2013. Timing and climatic drivers for glaciation across semi-arid western Himalayan–Tibetan orogen. Quat. Sci. Rev. 78, 188–208.
Ehlers, J., Gibbard, P.L., Hughes, P.D., 2011. Quaternary Glaciations—Extent and Chronology, vol. 15. A Closer Look. Elsevier, Amsterdam, pp. 1–1108.
Fabel, D., Harbor, J., Dahms, D., James, A., Elmore, D., Horn, L., Daley, K., Steele, C., 2004. Spatial patterns of glacial erosion at a valley scale derived from terrestrial cosmogenic ^{10}Be and ^{26}Al concentrations in rock. Ann. Assoc. Am. Geogr. 94, 241–255.
Fabel, D., Stroeven, A.P., Harbor, J., Kleman, J., Elmore, D., Fink, D., 2002. Landscape preservation under Fennoscandian ice sheets determined from in situ produced ^{10}Be and ^{26}Al. Earth Planet Sci. Lett. 201, 397–406.
Gosse, J.C., Phillips, F.M., 2001. Terrestrial in situ cosmogenic nuclides: theory and application. Quat. Sci. Rev. 20, 1475–1560.
Guo, W.Q., Liu, S.Y., Xu, J.L., Wu, L.Z., Shangguan, D.H., Yao, X.J., Wei, J.F., Bao, W.J., Yu, P.C., Liu, Q., Jiang, Z.L., 2015. The second Chinese glacier inventory: data, methods and results. J. Glaciol. 61, 357–372.
Herzschuh, U., 2006. Palaeo-moisture evolution in monsoonal Central Asia during the last 50,000 years. Quat. Sci. Rev. 25, 163–178.
Heyman, J., Applegate, P.J., Blomdin, R., Gribenski, N., Harbor, J.M., Stroeven, A.P., 2016. Boulder height- exposure age relationships from a global glacial ^{10}Be compilation. Quat. Geochronol. 34, 1–11.
Heyman, J., Stroeven, A.P., Harbor, J.M., Caffee, M.W., 2011. Too young or too old: evaluating cosmogenic exposure dating based on an analysis of compiled boulder exposure ages. Earth Planet Sci. Lett. 302, 71–80.
Hu, G., Yi, C.L., Liu, J.H., Wang, P., Zhang, J.F., Li, S.H., Li, D.H., Huang, J.W., Wang, H. Y., Zhang, A.M., Shi, L.F., Shui, X.J., 2020. Glacial advances and stability of the moraine dam on mount Namcha Barwa since the last glacial maximum, eastern himalayan syntaxis. Geomorphology 365, 107246.

Hu, G., Yi, C.L., Zhang, J.F., Dong, G.C., Liu, J.H., Xu, X.K., Jiang, T., 2017. Extensive glacial advances during the Last Glacial Maximum near the eastern Himalayan syntaxis. Quat. Int. 443, 1–12.
Hughes, P.D., Gibbard, P.L., Woodward, J.C., 2005. Quaternary glacial records in mountain regions: a formal stratigraphical approach. Episodes 28, 85–92.
Immerzeel, W.W., van Beek, L.P.H., Bierkens, M., 2010. Climate change will affect the Asian water towers. Science 328, 1382–1385.
IPCC, 2013. Climate Change 2013: the Physical Science Basis. Cambridge University Press, Cambridge, pp. 383–464.
Jakob, L., Gourmelen, N., Ewart, M., Plummer, P., 2021. Spatially and temporally resolved ice loss in High Mountain Asia and the Gulf of Alaska observed by CryoSat-2 swath altimetry between 2010 and 2019. Cryosphere 15, 1845–1862.
Jiao, K.Q., Iwata, S., 1993. Glacial changes since the last glaciation in kunlun pass, Tanggula pass and, southeastern xizang (Tibet) (in Chinese with English summary). In: Glaciological Climate and Environment on the Qing-Zang Plateau. Science Press, Beijing, pp. 120–129.
Jiao, K.Q., Zhang, Z.S., 1988. Glacier inventory of China VII: qinghai-xizang plateau interior area (drainage basins of the siling lake) (Chinese). In: Science Press, Beijing, pp. 1–73.
Kelly, M.A., Ivy-Ochs, S., Kubik, P.W., von Blanckenburg, F., Schlüchter, C., 2006. Chronology of deglaciation based on ^{10}Be dates of glacial erosional features in the Grimsel Pass region, central Swiss Alps. Boreas 35, 634–643.
Kohl, C.P., Nishiizumi, K., 1992. Chemical isolation of quartz for measurement of in-situ-produced cosmogenic nuclides. Geochem. Cosmochim. Acta 56, 3583–3587.
Lee, S.Y., Seong, Y.B., Owen, L.A., Murari, M.K., Lim, H.S., Yoon, H.I., Yoo, K.C., 2014. Late Quaternary glaciation in the Nun-Kun massif, northwestern India. Boreas 43, 67–89.
Li, B.Y., Li, J.J., Cui, Z.J., Zheng, B.X., Zhang, Q.S., Wang, F.B., Zhou, S.Z., Shi, Z.H., Jiao, K.Q., Kang, J.C., Advisor, Scientific, Shi, Y.F., 1991. Quaternary glacial distribution map of the qinghai-xizang (Tibet) plateau (1: 3000000) (Chinese and English). In: Science Press, Beijing, p. 1.
Li, J.J., Zheng, B.X., Yang, X.J., Xie, Y.Q., Zhang, L.Y., Ma, Z.H., Xu, S.Y., 1986. Glaciers of Xizang (in Chinese).. Science Press, Beijing, pp. 1–328.
Li, S.J., Li, S.D., 1992. Quaternary glacial and environmental changes in the region of Hoh Xil, Qinghai Province (in Chinese with English abstract). J. Glaciol. Geocryol. 14, 316–324.
Li, Y.K., Harbor, J., Stroeven, A.P., Fabel, D., Kleman, J., Fink, D., Caffee, M., Elmore, D., 2005. Ice sheet erosion patterns in valley systems in northern Sweden investigated using cosmogenic nuclides. Earth Surf. Process. Landforms 30, 1039–1049.
Li, Y.K., 2018. Determining topographic shielding from digital elevation models for cosmogenic nuclide analysis: a GIS model for discrete sample sites. J. Mt. Sci. 15, 939–947.
Lifton, N., Sato, T., Dunai, T.J., 2014. Scaling *in situ* cosmogenic nuclide production rates using analytical approximations to atmospheric cosmic-ray fluxes. Earth Planet Sci. Lett. 386, 149–160.
Lisiecki, L.E., Raymo, M.E., 2005. A Pliocene-Pleistocene stack of 57 globally distributed benthic δ^{18}O records. Paleoceanography 20, PA1003.
Liu, J.H., Yi, C.L., Li, Y.K., Bi, W.L., Zhang, Q., Hu, G., 2017. Glacial fluctuations around the Karola pass, eastern Lhagoi Kangri range, since the last glacial maximum. J. Quat. Sci. 32, 516–527.
Liu, S.Y., Yao, X.J., Guo, W.Q., Xu, J.L., Shangguan, D.H., Wei, J.F., Bao, W.J., Wu, L.Z., 2015. The contemporary glaciers in China based on the Second Chinese Glacier Inventory (in Chinese with English abstract). Acta Geograph. Sin. 70, 3–16.
Mix, A.C., Bard, E., Schneider, R., 2001. Environmental processes of the ice age: land, oceans, glaciers (EPILOG). Quat. Sci. Rev. 20, 627–657.
Murari, M.K., Owen, L.A., Dortch, J.M., Caffee, M.W., Dietsch, C., Fuchs, M., Haneberg, W.C., Sharma, M.C., Townsend-Small, A., 2014. Timing and climatic drivers for glaciation across monsoon-influenced regions of the Himalayan–Tibetan orogen. Quat. Sci. Rev. 88, 159–182.
Nishiizumi, K., Imamura, M., Caffee, M.W., Southon, J.R., Finkel, R.C., McAninch, J., 2007. Absolute calibration of ^{10}Be AMS standards. Nucl. Instrum. Methods Phys. Res., Sect. B 258, 403–413.
Nishiizumi, K., Winterer, E.L., Kohl, C.P., Klein, J., Middleton, R., Lal, D., Arnold, J.R., 1989. Cosmic ray production rates of ^{26}Al and ^{10}Be in quartz from glacially polished rocks. J. Geophys. Res. 94, 17907–17915.
Owen, L.A., Dortch, J.M., 2014. Nature and timing of Quaternary glaciation in the Himalayan-Tibetan orogen. Quat. Sci. Rev. 88, 14–54.
Owen, L.A., Finkel, R.C., Barnard, P.L., Ma, H.Z., Asahi, K., Caffee, M.W., Derbyshire, E., 2005. Climatic and topographic controls on the style and timing of late Quaternary glaciation throughout Tibet and the Himalaya defined by ^{10}Be cosmogenic radionuclide surface exposure dating. Quat. Sci. Rev. 24, 1391–1411.
Peng, X., Chen, Y.X., Li, Y.K., Liu, B.B., Liu, Q., Yang, W.L., Cui, Z.J., Liu, G.N., 2020. Late Holocene glacier fluctuations in the Bhutanese Himalaya. Global Planet. Change 187, 103137.
Peng, X., Chen, Y.X., Liu, G.N., Liu, B.B., Li, Y.K., Liu, Q., Han, Y.S., Yang, W.L., Cui, Z.J., 2019. Late quaternary glaciations in the Cogarbu valley, Bhutanese Himalaya. J. Quat. Sci. 34, 40–50.
Porter, S.C., 2001. Snowline depression in the tropics during the last glaciation. Quat. Sci. Rev. 20, 1067–1091.
Pu, J.C., 1994. Glacier Inventory of China VIII: the Changjiang (Yangtze) River Drainage Basin (in Chinese).. Gansu Culture Press, Lanzhou, pp. 1–142.
Reuther, A.U., Fiebig, M., Ivy-Ochs, S., Kubik, P.W., Reitner, J.M., Jerz, H., Heine, K., 2011. Deglaciation of a large piedmont lobe glacier in comparison with a small mountain glacier– new insight from surface exposure dating. Two studies from SE Germany. E&G Quaternary Science Journal 60, 248–269.
Rowan, A.V., 2017. The 'Little Ice Age' in the Himalaya: a review of glacier advance driven by Northern Hemisphere temperature change. Holocene 27, 292–308.
Saha, S., Owen, L.A., Orr, E.N., Caffee, M.W., 2018. Timing and nature of Holocene glacier advances at the northwestern end of the Himalayan-Tibetan orogen. Quat. Sci. Rev. 187, 177–202.
Saha, S., Owen, L.A., Orr, E.N., Caffee, M.W., 2019. High-frequency Holocene glacier fluctuations in the Himalayan-Tibetan orogen. Quat. Sci. Rev. 220, 372–400.
Schaefer, J.M., Oberholzer, P., Zhao, Z.Z., Ivy-Ochs, S., Wieler, R., Baur, H., Kubik, P.W., Schlüchter, C., 2008. Cosmogenic beryllium-10 and neon-21 dating of late Pleistocene glaciations in Nyalam, monsoonal Himalayas. Quat. Sci. Rev. 27, 295–311.
Schäfer, J.M., Tschudi, S., Zhao, Z.Z., Wu, X.H., Ivy-Ochs, S., Wieler, R., Baur, H., Kubik, P.W., Schlüchter, C., 2002. The limited influence of glaciations in Tibet on global climate over the past 170000 yr. Earth Planet Sci. Lett. 194, 287–297.
Seong, Y.B., Owen, L.A., Yi, C., Finkel, R.C., 2009. Quaternary glaciation of Muztag Ata and Kongur Shan: evidence for glacier response to rapid climate changes throughout the late glacial and Holocene in westernmost Tibet. Geol. Soc. Am. Bull. 121, 348–365.
Shi, Y.F., Cui, Z.J., Su, Z., 2006. The Quaternary Glaciations and Environmental Variations in China (In Chinese with English Summary). Hebei Science and Technology Publishing House, Shijiazhuang, pp. 1–618.
Shi, Y.F., Yu, G., Liu, X.D., Li, B.Y., Yao, T.D., 2001. Reconstruction of the 30-40 ka BP enhanced Indian monsoon climate based on geological records from the Tibetan Plateau. Palaeogeogr. Palaeoclimatol. Palaeoecol. 169, 69–83.
Shi, Y.F., Zhao, J.D., Wang, J., 2011. New Understanding of Quaternary Glaciations in China (in Chinese).. Shanghai Popular Science Press, Shanghai, pp. 1–213.
Shi, Y.F., Zheng, B.X., Yao, T.D., 1997. Glaciers and environments during the last glacial maximum (LGM) on the Tibetan plateau (in Chinese with English abstract). J. Glaciol. Geocryol. 19, 97–113.
Thompson, L.G., Mosley-Thompson, E., Brecher, H., Davis, M., León, B., Les, D., Lin, P.N., Mashiotta, T., Mountain, K., 2006. Abrupt tropical climate change: past and present. Proc. Natl. Acad. Sci. USA 103, 10536–10543.
Thompson, L.G., Yao, T., Davis, M.E., Henderson, K.A., Mosley-Thompson, E., Lin, P.N., Beer, J., Synal, H.A., Cole-Dai, J., Bolzan, J.F., 1997. Tropical climate instability: the last glacial cycle from a Qinghai-Tibetan ice core. Science 276, 1821–1825.
Wang, J., Wang, W.C., Cao, B., Cui, H., Chen, X.J., Qiu, J.K., Lei, M.H., Liao, J.S., 2023. Millennial-scale glacier fluctuations on the southeastern Tibetan Plateau during MIS 2. Earth Planet Sci. Lett. 601, 117903.
Wang, J., Zhou, S.Z., Tang, S.L., Colgan, P.M., Munroe, J.S., 2007. The sequence of Quaternary glaciations around the Tanggula Pass (in Chinese with English abstract). J. Glaciol. Geocryol. 29, 149–155.
Wang, Y.J., Cheng, H., Edwards, R.L., Kong, X.G., Shao, X.H., Chen, S.T., Wu, J.Y., Jiang, X.Y., Wang, X.F., An, Z.S., 2008. Millennial- and orbital-scale changes in the East Asian monsoon over the past 224000 years. Nature 1090–1093.
Xu, X.K., Yi, C.L., 2014. Little ice age on the Tibetan Plateau and its bordering mountains: evidence from moraine chronologies. Global Planet. Change 116, 41–53.
Yao, T.D., Thompson, L., Yang, W., Yu, W.S., Gao, Y., Guo, X.J., Yang, X.X., Duan, K.Q., Zhao, H.B., Xu, B.Q., Pu, J.C., Lu, A., Xiang, Y., Kattel, D.B., Joswiak, D., 2012. Different glacier status with atmospheric circulations in Tibetan Plateau and surroundings. Nat. Clim. Change 2, 663–667.
Zech, R., 2012. A late Pleistocene glacial chronology from the Kitschi-Kurumdu Valley, Tien Shan (Kyrgyzstan), based on ^{10}Be surface exposure dating. Quat. Res. 77, 281–288.
Zech, R., Glaser, B., Sosin, P., Kubik, P.W., Zech, W., 2005. Evidence for long-lasting landform surface instability on hummocky moraines in the Pamir Mountains (Tajikistan) from ^{10}Be surface exposure dating. Earth Planet Sci. Lett. 237, 453–461.
Zhang, L.Y., 1981. Glaciers at the source region of Tuotuo River in the upper reaches of the Changjiang and their evolution (in Chinese with English abstract). J. Glaciol. Cryopedol. 3, 1–9.
Zhang, Q., Yi, C.L., Dong, G.C., Fu, P., Wang, N.L., Capolongo, D., 2018. Quaternary glaciations in the lopu Kangri area, central Gangdise mountains, southern Tibetan plateau. Quat. Sci. Rev. 201, 470–482.
Zhang, W., Liu, L., Chen, Y.X., Liu, B.B., Harbor, J.M., Cui, Z.J., Liu, R., Liu, X., Zhao, X., 2016. Late glacial ^{10}Be ages for glacial landforms in the upper region of the Taibai glaciation in the Qinling Mountain range, China. J. Asian Earth Sci. 115, 383–392.
Zhao, J.D., Harbor, J.M., Qiu, J.K., Caffee, M.W., Guo, W.Q., Ji, H.H., Liu, R.L., Ma, H.N., 2023a. Glacier fluctuations since the global last glacial maximum in the eastern Tanggula mountains, China. Palaeogeogr. Palaeoclimatol. Palaeoecol. 627, 111742.
Zhao, J.D., Liu, R.L., Wang, W.C., Dong, Z.J., Qiu, J.K., Zhang, Y.N., Luo, C.W., 2021. Terrestrial in situ cosmogenic nuclides (TCN) dating targets preparation: a case study of its application in Quaternary glaciations research (In Chinese with English abstract). J. Glaciol. Geocryol. 43, 767–775.
Zhao, J.D., Qiu, J.K., Harbor, J.M., Ji, H.H., Caffee, M.W., Guo, W.Q., Zheng, H.J., 2023b. Timing and extent of late Quaternary glaciations on Karlik Mountain, eastern Tianshan range, China. Quat. Sci. Rev. 306, 108038.
Zhao, J.D., Shi, Y.F., Wang, J., 2011. Comparison between Quaternary glaciations in China and the marine oxygen isotope stage (MIS): an Improved Schema (in Chinese with English abtract). Acta Geograph. Sin. 66, 867–884.